VIII International Conference on Particle-Based Methods
PARTICLES 2023
U. Perego, M. Cremonesi, A. Franci (Eds)

A DEM-FEM COUPLING FRAMEWORK APPLIED TO RAILROAD INFRASTRUCTURE SIMULATIONS

Anita Ullrich[1], Johannes Quist[1], Christoffer Cromvik[1], Klas Jareteg[2], Adam Bilock[2] and Fredrik Edelvik[1]

[1] Fraunhofer-Chalmers Centre (FCC)
Chalmers Science Park, SE-412 88 Gothenburg, Sweden
e-mail: anita.ullrich@fcc.chalmers.se, www.fcc.chalmers.se

[2] IPS Particle Technology AB
Sven Hultins gata 9, SE-412 58 Gothenburg, Sweden
www.industrialpathsolutions.com

Abstract: Swedish and other European governments invest significant resources in railroad infrastructure, including maintenance and construction. The degradation of track ballast layers is one of the most critical maintenance issues. Hence, it is of significant interest for infrastructure owners to find novel solutions to mitigate the problem by improving design and maintenance operations. However, established tools for the simulation of railroad systems typically consider the ballast as a solid continuum structure, while in practice, the discrete nature of the particle assembly has to be accurately represented in the model. The sleepers and rails must be modelled as solid structures, which results in the complex coupled problem of combining particulate and structural analysis models.

In this paper, the simulation of railroad infrastructure with the example of a transition zone is performed with an explicit surface coupling algorithm of the Discrete Element Method (DEM) and the Finite Element Method (FEM). The ballast layer is represented by individual particles in DEM, where the computations are performed on the GPU. This study focuses on the comparison between a convex and a non-convex particle shape. The rail system with sleepers and the subground with varying stiffness is modelled with solid structures in FEM.

Properties of the ballast bed, such as the particle shape, are found to have a significant impact on the stiffness within the bed and the deflection of the sleepers and rails. Furthermore, the sudden transition from low to high stiffness causes a peak in tensile stress in the subground. The results show that accurate particle shape representation and high computational performance are critical aspects of achieving predictions on a relevant scale. Studying the ballast layer as a particulate system provides a new perspective on dynamics in tracked ballast structures.

Keywords. DEM, FEM, Non-convex particles, Railroad simulations, Coupling

1 INTRODUCTION

Railroad infrastructure is critical for a sustainable transport system. Sweden has the objective to develop a climate-neutral transport system until 2050 [1]. Nowadays, the Swedish Transport Administration is responsible for 14,000 km railroad tracks, which lead to an annual operating and maintenance cost of circa 500 million EUR [2]. To enable Sweden to reach its sustainability goals includes the construction of railway structures with optimal performance and durability. Part of the optimisation is to analyse existing railroad structures and apparent problems that cause frequent maintenance operations. Understanding the current problems is fundamental for the search for new solutions that can be implemented in new railroad tracks. The dynamics inside the ballast layer must be understood to fully understand the dynamics in railroad tracks. Thus, efficient simulation methods combining the modelling of the solid structures, such as sleepers, rails and sublayers in the track system, and particle systems, which can represent the ballast layer, are required.

Common simulation methods for railroad structures are the Finite Element Method (FEM) and the Discrete Element Method (DEM) [3]. Sysyn et al. [4] utilise FEM to investigate the railway settlement with ballast voids. Jing et al. [5] apply DEM to model the interactions between hanging sleepers and the ballast layer. While FEM captures the macroscopic ballast behaviour and the dynamics of the solid structures, DEM can resolve the ballast layer on a microscopic level. However, DEM is more computationally demanding than FEM. The coupling of both simulation methods can efficiently model the complete railway system.

Kaewunruen and Mirza [6] model a railway bridge with a hybrid discrete-finite element simulation. Wang et al. [7] utilise a multi-scale DEM-FEM coupling to simulate high-speed railways. Song et al. [8] apply a DEM-FEM coupling to simulate a single sleeper on a ballast bed under cyclic loading and evaluate the resulting pressure distribution.

Chen and McDowell [9] approach the simulation of transition zones with 3D DEM and a multisphere model to represent the particles. They investigate both a single step and multi step-by-step change for the subgrade stiffness distribution and apply a cyclic loading on each sleeper with a time offset from sleeper to sleeper. Liu et al. [10] simulate welded rail positions with a FEM model. Nasrollahi et al. [11] utilise a non-linear FEM model to study the influence of higher axle loads and under sleeper pads on sleeper settlement while applying a static force as load. Sakhare et al. [12] perform a 2D plane-strain FE analysis to investigate the influence of parameters such as the approach slab geometry, backfill soil type as well as the direction of train movement and train speed with a load pattern that follows support functions at each rail node. Shi et al. [13] and Shi and Chen [14] performed a DEM-FDM simulation where DEM models the ballast and sleepers and FDM models the subground to evaluate different transition section forms and the influence of under sleeper pads.

According to Alabbasi and Hussein [3], the modelled particle shape should be as close to the real shape as possible for realistic results. A common approach is the representation of particles with multispheres [15, 16]. Lu and McDowell [16] found a difference in the

ballast settlement in railway simulations between sphere and multi-sphere particle models. The results suggest more interlocking between the clumps than the spheres. Further, polyhedral particle models were used to model realistic particle shapes [17]. However, the contact detection is time extensive [3] due to the geometrical complexity and determination of particle overlaps. Convex polyhedra are an efficient approximation of polyhedral particles [18, 19], where the difficulties that arise with polyhedral shapes can be overcome. Ji et al. [20] applied the dilated polyhedron model for railroad ballast simulations as well as Eliáš [21], who found that the inclusion of particle breakage increases the accuracy of the simulation results.

For this study, a previously developed DEM-FEM surface coupling is used [22]. In this implementation, a state-of-art explicit DEM solver Demify®, with a C++ backend and Python interface, is applied for the ballast particle simulations. Demify® has been applied for large scale road infrastructure research [23, 24] and the computations are performed on the GPU [25]. The solid structures are modelled with an implicit FEM method with the Bossak-Newmark algorithm [26], which includes artificial damping. Following the classification of Stransky [27], the applied coupling model is a surface DEM-FEM coupling and was verified and validated [22]. Furthermore, the coupling was previously applied to railroad infrastructure simulations for the case of a single sleeper on a ballast bed loaded with a cycling load pattern [22] and the simulation of a three-sleeper-segment on a trough bridge loaded with a static load [28]. This study demonstrates the impact of realistic particle shapes for railroad simulations by comparing the results for convex and non-convex particle models. The dilated polyhedron model is chosen to represent convex ballast material particles. To conquer the geometrical complexity of non-convex particles, the non-convex shapes are modelled by combining several dilated polyhedra into one compound shape. Benchmarks are performed to show the efficiency of the simulations, especially regarding the simulation of non-convex particles as compounds of convex particles.

2 TRANSITION ZONE SIMULATION CASE

The load pattern in Figure 1 is derived from load model 71 in [29] and applied on each rail node varying over time as indicated with the visualisation of different timestamps. 50 % of the maximum load is applied on rail nodes with a distance of 1.6 m to each other, corresponding to the axle distance. With a rail element length of 0.1 m, this corresponds to each 16th node. Each adjacent rail node of those receives 25 % of the maximum load. With the given axle distance and a train speed of 10 m/s, one load cycle has a duration of 0.16 s.

The subground, rails and sleepers are modelled as FEM objects and their surface triangulations are transferred to DEM for the coupling to the particle system. Rails and sleepers are tetrahedral meshes with an element length of 0.1 m. The subground is modelled as a hexahedral mesh with an element length of 0.2 m. As only a section of a railway track is modelled in this case, symmetry boundary conditions on the ends of the rail mesh are set to model the connection to the rest of the track. The symmetry is applied in X and Y direction at the red positions indicated in Figure 4. The subground

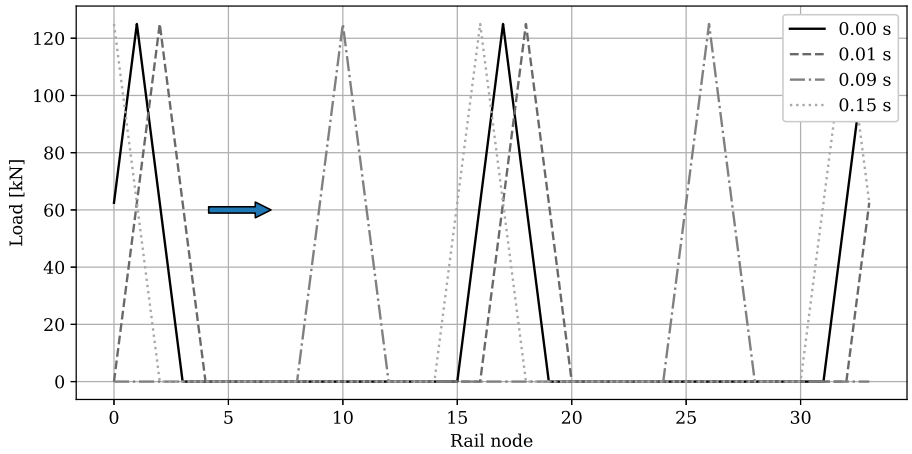

Figure 1: A dynamic load pattern illustrated for an axle distance of 1.6 m and an axle total load of 250 kN after 0, 0.01, 0.09 and 0.15 seconds into the simulation for 30 rail nodes with a horizontal distance of 0.1 m. The arrow indicates the load movement direction.

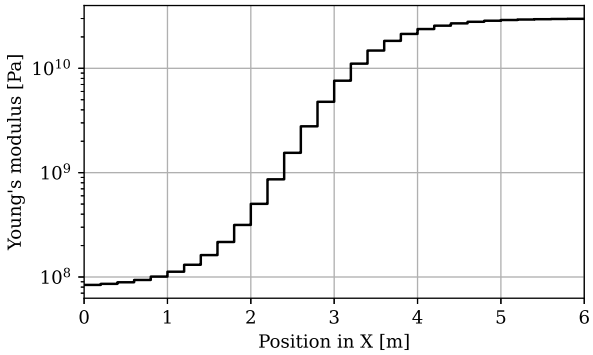

Figure 2: Transient of Young's modulus for the subground varied element-wise across the X domain.

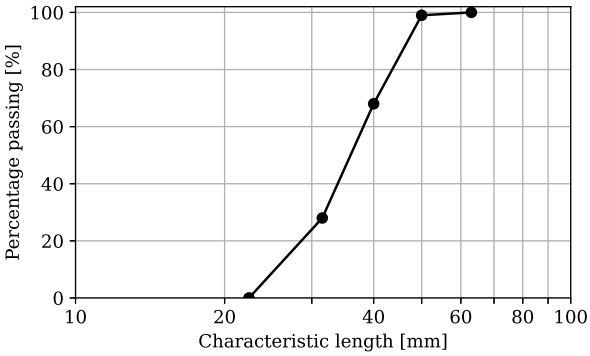

Figure 3: Size distribution of particles in the ballast bed with a minimal size of 22.4 mm and a maximal size of 63 mm.

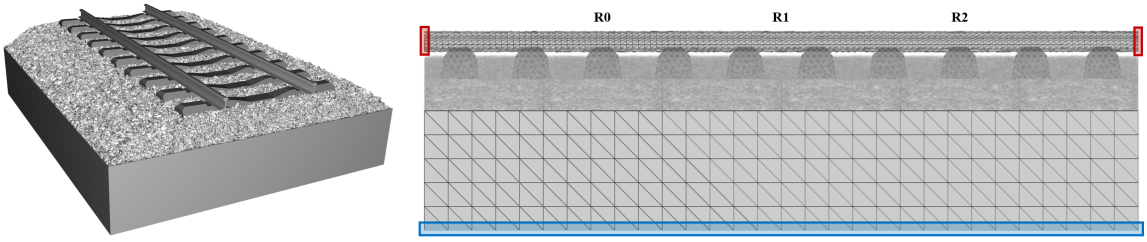

Figure 4: Overview of the simulation case with an illustration of the position of the boundary conditions on rails (red) and subground (blue).

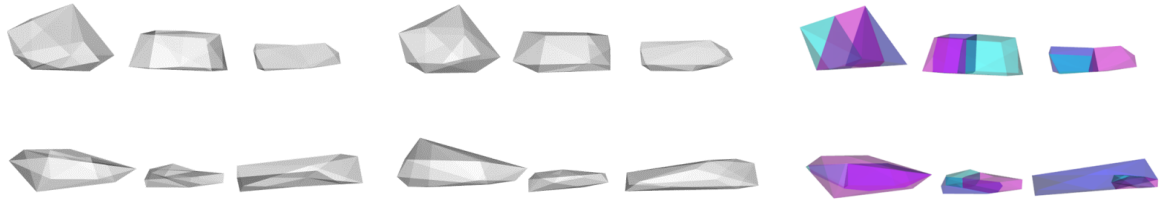

(a) Simplified rock model scans (b) Convex rock models (c) Compound rock models

Figure 5: The simplified original rock scans and the particle shapes used in the simulations as convex polyhedra and non-convex compound polyhedra.

bottom (blue) is fixated with a clamp boundary condition. The stiffness applied to the subground varies across the X domain to model the transition zone, and the stiffness transient is given in Figure 2. The ballast layer is simulated as a particle system with rock-shaped particles with DEM. The size distribution of the ballast material is given in Figure 3 and corresponds to Category A according to Swedish Standards [30].

Simplified scans of six different rocks (Figure 5a) serve as a basis for the simulated particle shapes. Convex approximations of the scans define convex dilated polyhedra (20 triangles each, Figure 5b) and convex decompositions of the scans into three sub-meshes (10-30 triangles each,Figure 5c) which combined represent a non-convex particle consisting of convex dilated polyhedra (60 triangles each). The decomposition is performed with the approximate convex decomposition algorithm for 3D meshes presented in [31].

The preparation of the simulation domain is performed in several steps. First, an initial cell of dimensions $1 \times 1 \times 1$ m filled with rock particles is generated. This cell is then utilised for a volume-filling method to fill the ballast bed's whole volume, which is based on Swedish standards [32]. The sleeper system, including rails, is placed on top and positioned in a pure DEM simulation such that the contact force between the sleeper system and the particles corresponds to the gravitational force acting on the sleeper system. This simulation state is saved for each configuration and initialises all further simulations.

All parameters and their values of the simulation configuration are listed in Table 1. A convergence study regarding the timestep resolution has been performed with the result that a DEM timestep of 1×10^{-6} s and a FEM timestep of 1×10^{-5} s are small enough to obtain stable simulations for the given parameter configuration. To investigate the stability of the coupling for the case of transition zones and to evaluate the importance of particle shape, the simulations were sped up by reducing the stiffness of the ballast particles. Thus, the Young's modulus of the ballast particles was reduced to 1 GPa, whereas the realistic Young's modulus for granite is approximately 50 GPa [33]. A new stability study would be required for stiffer particles, resulting in smaller timesteps. Thus, the reduced stiffness needs to be considered when evaluating this study's results, e.g. the track system deflection is expected to be larger than for a realistic ballast bed stiffness. However, that choice does not diminish the findings of this study regarding the impact of a non-convex particle shape.in [31].

Parameter	Value	Unit
Tet mesh element length	0.1	m
Hex mesh element length	0.2	m
Particle density	2700.0	kg/m^3
Particle Young's modulus	1×10^9	Pa
Particle Poisson's ratio	0.27	-
Particle-particle friction	0.6	-
Particle-particle restitution	0.2	-
Subground density	3000.0	kg/m^3
Subground Young's modulus	$[8 \times 10^7, 3 \times 10^{10}]$	Pa
Subground Poisson's ratio	0.3	-
Subground dimensions (L,W,H)	6.0, 4.85, 1.0	m
Sleeper density	2548.42	kg/m^3
Sleeper Young's modulus	3.7×10^{10}	Pa
Sleeper Poisson's ratio	0.2	-
Rail density	7858.0	kg/m^3
Rail Young's modulus	20×10^{10}	Pa
Rail Poisson's ratio	0.2	-
Particle-object friction	0.6	-
Particle-object restitution	0.2	-
DEM timestep	1×10^{-6}	s
FEM/Coupling timestep	1×10^{-5}	s
Train speed	10.0	m/s
Axle load	250	kN
Axle distance	1.6	m

Table 1: Simulation configuration.

3 RESULTS

All results are the mean of three simulations with the same configuration and a pale band showing the standard deviation. The red curve corresponds to the simulations with simple dilated polyhedral particle models (D), and the blue curve represents the simulations with the dilated polyhedral compounds (CD).

The peak tensile and compressive stress in the subground across the X domain during the complete simulation can be seen in Figure 6. A significant result is that the stresses are similar for both particle representations. Furthermore, the tensile stresses show a clear peak in the middle of the domain with a stress of 0.1 MPa, corresponding to the steepest transition in stiffness of the subground. The compressive stress increases significantly at the steepest transition and stays on a similar level before and after the transition. The positions of the spikes in the results coincide with the positions of the sleepers, which have a distance of 0.6 m to each other.

In Figure 7, the maximal deflection in all sleepers over time and in Figure 8, the mean

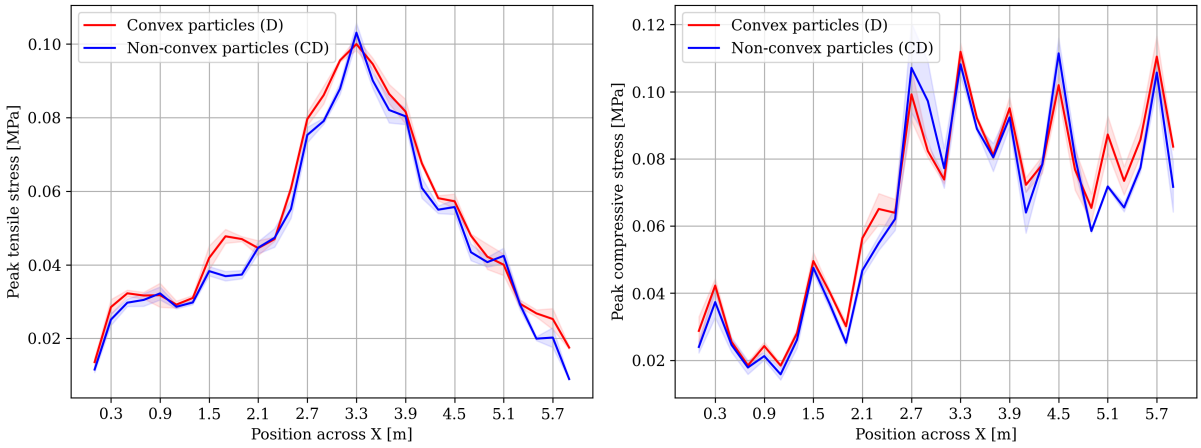

(a) Peak tensile stress in the subground across the X domain during the simulation.

(b) Peak compressive stress in the subground across the X domain during the simulation.

Figure 6: Peak tensile and compressive stress in the subground during the simulation.

deflection in the three reference positions in the rails are shown. Both results show a notable decrease in deflection for model CD. While both curves for the sleeper deflection start with a similar deflection, corresponding to the sleeper system's initial settlement onto the ballast bed, they diverge over time. After 8 seconds, the deflection for model CD is approximately 5 mm smaller than for model D. Regarding the rail deflection, this observation is more distinct. In this case, both curves start again with a similar deflection, and after 8 seconds, the deflection for model CD is approximately 7 mm for R0, 9 mm for R1 and 7 mm for R2 smaller than for model D. The deflection in R0 and R2 are slightly larger than in R1, with a difference of approximately 2.5 mm after 8 seconds. Another aspect both figures have in common is a lower variance in the simulations with model CD.

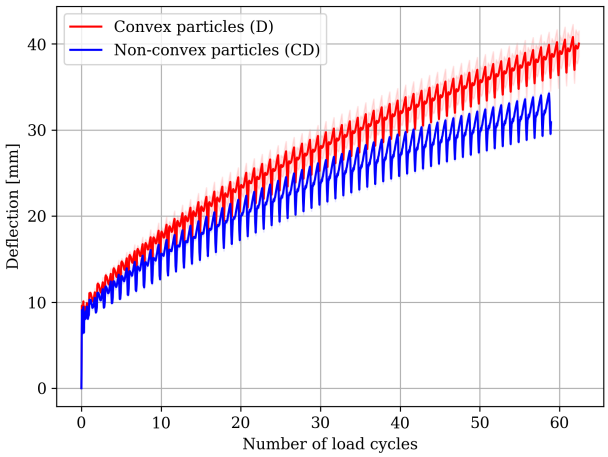

Figure 7: Maximal deflection in the sleepers.

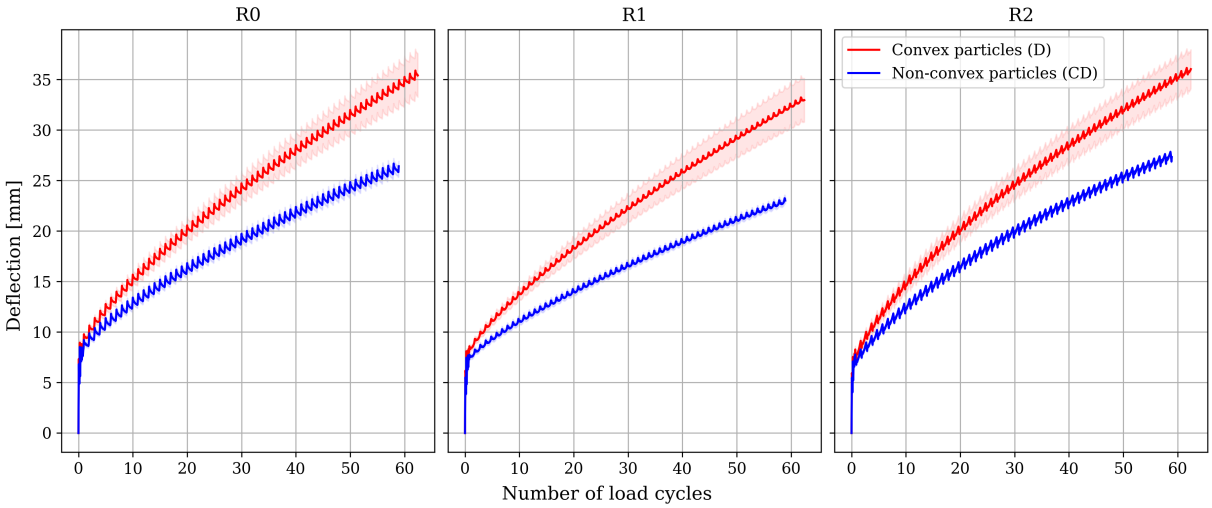

Figure 8: Mean deflection in the rail reference positions R0, R1 and R2.

# FEM Elements	# Particles	Particle Model	Total	DEM	FEM	Coupling
3.5×10^4	3.3×10^5	D	303	85	122	96
1.2×10^5	3.3×10^5	D	658	88	344	225
3.5×10^4	3.4×10^5	CD	495	256	144	95
1.2×10^5	3.4×10^5	CD	875	260	378	236

Table 2: Benchmark of a varying FEM object resolution and DEM particle model type. The simulated time was 0.5 seconds, and the given times in the table are the computational time in minutes.

As the deflection results suggested, the effective bed stiffness in Figure 9 supports the observation that the ballast bed has a higher effective stiffness for model CD. For both models, the results indicate a convergence of the effective bed stiffness. The effective bed stiffness for model CD settles around 540 MPa, whereas it settles around 430 MPa for model D.

The effect on the ballast bed can be observed in Figure 10, where a histogram of the total force over the whole particle population over all sampling steps is visualised. For a total force up to 1 kN, the share of particles experiencing the force is similar between model C and model CD. However, the histogram for model CD measures forces up to 12 kN, whereas the maximal measured force for model D is around 1.5 kN. Only a fraction of the particles experience a higher force than 1.5 kN for model CD. However, the simulation captured a time window of approximately 9 s. This fraction could yield significant damage to the ballast bed in long-term usage.

To evaluate the efficiency and applicability of the coupled simulation, a benchmark is performed on a machine with a Xeon Gold 6134 CPU and a NVIDIA V100 GPU. For the benchmark, 0.5 s of the transition zone case is simulated over five runs, for which the average times are evaluated. The benchmark is performed for two different FEM object

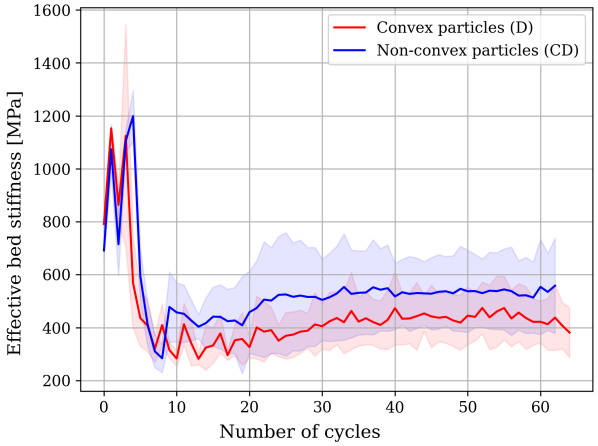

Figure 9: Effective bed stiffness in the ballast bed based on the slopes of the sleeper stress-strain curve.

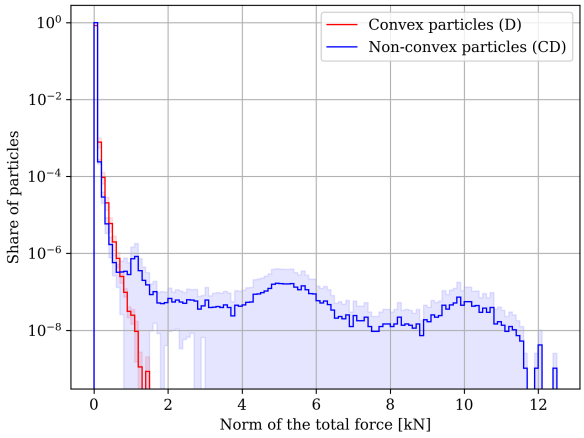

Figure 10: Histogram of total force acting on all particles over all sampling steps.

resolutions, affecting the number of elements and the two different particle models (D and CD). The resolution with 3.5×10^4 elements in the FEM objects is the one stated in the simulation configuration. The benchmark results are given in minutes in Table 2.

The fastest simulation is the one with model D and a lower FEM object resolution with a total time of 5 hours. In this case, the DEM simulation is faster than the FEM simulation and the coupling operations, demonstrating the GPU implementation's efficiency. When comparing the cases with model D and CD, the results show, as expected, an increase by a factor of 3 in the DEM computational time, whereas the time for FEM and the coupling are similar to the case with model D. A factor 3 is expected since the compound dilated model consists of 3 submodels. Considering the increase in the resolution of the FEM objects by a factor of 3.4, the time for the FEM simulation increases by a factor of 2.8 for D and 2.6 for CD. Furthermore, the measured time for the coupling operations increases by a similar factor for both models since all information transfer between DEM and FEM are the forces acting on the FEM nodes or their displacements. Thus, the required time scales in size with the number of FEM elements.

4 CONCLUSION

From the obtained results, we can conclude that

- The applied DEM-FEM coupling enables us to simulate railway transition zones efficiently.
- Non-convex particles cause a lower settlement of sleepers and rails in this simulation case and a higher effective bed stiffness. Furthermore, the measured forces in the particle population are significantly higher than for the convex particles.
- The results show that the sudden transition causes a peak in the tensile and a sudden increase in the compressive stress in the subground.

- Valuable information, such as a force histogram over the particle population, can be obtained with the simulations that cannot be evaluated from experiments.
- The deflection results are larger than they would appear in reality, thus further studies for the compaction of the ballast bed and a more realistic particle stiffness are needed to obtain more realistic results.

Aspects for future work are

- The extension of the DEM-FEM coupling with multibody dynamics (MBD) for the simulation of trains or maintenance vehicles.
- A study of different stiffness transition functions with an optimisation regarding the effects on the ballast bed and solid structures, e.g. the tensile and compressive stress in the subground.
- Perform field measurements and compare the simulations to the experimental results.
- The inclusion of a particle breakage model in the simulation. The force distribution across the population presented in this study can serve as a basis to investigate the proportion of particles suspended to fracture in the transition zone. Additionally, it would be interesting to examine if the higher forces measured for model CD appear focused in a specific part of the bed, e.g. under the sleepers.

5 ACKNOWLEDGEMENTS

The authors acknowledge the financial support provided by the strategic innovation programme InfraSweden2030, a joint effort of Sweden's Innovation Agency (Vinnova), the Swedish Research Council (Formas) and the Swedish Energy Agency (Energimyndigheten).

REFERENCES

[1] Tågoperatörerna. *Järnväg 2050 En vision om järnvägens framtida roll i samhället.* 2019. URL: https://www.almega.se/app/uploads/sites/9/2019/11/bto-jarnvag2050.pdf (visited on 03/29/2022).

[2] Trafikverket. *Underhåll av väg och järnväg.* 2021. URL: https://www.trafikverket.se/resa-och-trafik/underhall-av-vag-och-jarnvag/ (visited on 03/29/2022).

[3] Y. Alabbasi et al. "Geomechanical Modelling of Railroad Ballast: A Review". In: *Archives of Computational Methods in Engineering* 28.3 (2019), pages 815–839. DOI: 10.1007/s11831-019-09390-4.

[4] M. Sysyn et al. "Mechanism of Sleeper–Ballast Dynamic Impact and Residual Settlements Accumulation in Zones with Unsupported Sleepers". In: *Sustainability* 13.14 (2021), page 7740. DOI: 10.3390/su13147740.

[5] G. Jing et al. "Micro-analysis of hanging sleeper dynamic interactions with ballast bed". In: *Journal of Vibroengineering* 17.1 (2015), pages 444–454.

[6] S. Kaewunruen et al. "Hybrid Discrete Element - Finite Element Simulation for Railway Bridge-Track Interaction". In: *IOP Conference Series: Materials Science and Engineering* 251 (2017), page 012016. DOI: 10.1088/1757-899x/251/1/012016.

[7] X. Wang et al. "Modeling of Coupling Mechanism between Ballast Bed and Track Structure of High-Speed Railway". In: *Mathematical Problems in Engineering* 2020 (2020), pages 1–12. DOI: 10.1155/2020/9768904.

[8] W. Song et al. "Interaction between Railroad Ballast and Sleeper: A DEM-FEM Approach". In: *International Journal of Geomechanics* 19.5 (2019), page 04019030. DOI: 10.1061/(asce)gm.1943-5622.0001388.

[9] C. Chen et al. "An investigation of the dynamic behaviour of track transition zones using discrete element modelling". In: *Proceedings of the Institution of Mechanical Engineers, Part F: Journal of Rail and Rapid Transit* 230.1 (2014), pages 117–128. DOI: 10.1177/0954409714528892.

[10] X. Liu et al. "Transient dynamics of a full wheel rail set passing a weld irregularity at high speed". In: *Engineering Failure Analysis* 148 (2023), page 107203. DOI: 10.1016/j.engfailanal.2023.107203.

[11] K. Nasrollahi et al. "Prediction of long-term differential track settlement in a transition zone using an iterative approach". In: *Engineering Structures* 283 (2023), page 115830. DOI: 10.1016/j.engstruct.2023.115830.

[12] A. Sakhare et al. "Dynamic behaviour of integral abutment bridge transition under moving train loads". In: *Transportation Geotechnics* 40 (2023), page 100989. DOI: 10.1016/j.trgeo.2023.100989.

[13] C. Shi et al. "Macro-meso dynamic analysis of railway transition zone: Hybrid DEM/FDM simulation and experimental validation". In: *Soil Dynamics and Earthquake Engineering* 135 (2020), page 106191. DOI: 10.1016/j.soildyn.2020.106191.

[14] C. Shi et al. "Coupled DEM/FDM to evaluate track transition stiffness under different countermeasures". In: *Construction and Building Materials* 266 (2021), page 121167. DOI: 10.1016/j.conbuildmat.2020.121167.

[15] C. Coetzee. "Calibration of the discrete element method and the effect of particle shape". In: *Powder Technology* 297 (2016), pages 50–70. ISSN: 0032-5910. DOI: https://doi.org/10.1016/j.powtec.2016.04.003. URL: http://www.sciencedirect.com/science/article/pii/S0032591016301620.

[16] M. Lu et al. "The importance of modelling ballast particle shape in the discrete element method". In: *Granular Matter* 9.1 (2006), page 69. ISSN: 1434-7636. DOI: 10.1007/s10035-006-0021-3. URL: https://doi.org/10.1007/s10035-006-0021-3.

[17] N. Govender et al. "Industrial scale particle simulations on the GPU using the Blaze-DEM code". In: *Proceedings of the 7th International Conference on Discrete Element Methods*. Springer. 2017, pages 1379–1388.

[18] B. Nye et al. "Intersecting dilated convex polyhedra method for modeling complex particles in discrete element method". In: *International Journal for Numerical and*

Analytical Methods in Geomechanics 38.9 (2014), pages 978–990. DOI: 10.1002/nag.2299.

[19] B. Nassauer et al. "Polyhedral particles for the discrete element method". In: *Granular Matter* 15.1 (2012), pages 85–93. DOI: 10.1007/s10035-012-0381-9.

[20] S. Ji et al. "Discrete Element Modeling of Rock Materials with Dilated Polyhedral Elements". In: *Procedia Engineering* 102 (2015), pages 1793–1802. DOI: 10.1016/j.proeng.2015.01.316.

[21] J. Eliáš. "Simulation of railway ballast using crushable polyhedral particles". In: *Powder Technology* 264 (2014), pages 458–465.

[22] A. Ullrich. "Development of a DEM-FEM framework for infrastructure simulations". Master's thesis. University of Gothenburg, 2022.

[23] J. Quist et al. *segregering av bergmaterialvid avlastning - fullskaliga försök för dem validering och undersökning avsegregering.* Technical report. Fraunhofer-Chalmers Research Centre, 2019.

[24] J. Quist et al. *Investigation of the effect of size segregation on roller compaction of unbound materials.* Technical report. Fraunhofer-Chalmers Centre for Industrial Mathematics, Computational Engineering & Design. Gothenburg, 2021.

[25] A. Bilock. "A GPU Polyhedral Discrete Element Method". Master's thesis. Chalmers University of Technology, 2020.

[26] W. Wood et al. "An alpha modification of Newmark's method". In: *International journal for numerical methods in engineering* 15.10 (1980), pages 1562–1566.

[27] J. Stransky. "Open Source DEM-FEM Coupling". In: *Particle-Based Methods III: Fundamentals and Applications.* 3rd International Conference on Particle-based Methods. 2013, 46–57. ISBN: 978-84-941531-8-1.

[28] A. Eriksson et al. "Numerical and Analytical Evaluation of Load Distribution Patterns on Ballasted Concrete Railway Bridges". In: *Building for the Future: Durable, Sustainable, Resilient: Proceedings of the fib Symposium 2023-Volume 2.* Springer Nature Switzerland, 2023, pages 109–118. DOI: 10.1007/978-3-031-32511-3_12.

[29] SIS. *Eurocode 1: Actions on structures - Part 2: Traffic loads on bridges.* Sweidsh Institute for Standards. 2003.

[30] SIS. *Aggregates for railway ballast.* Sweidsh Institute for Standards. 2003.

[31] X. Wei et al. "Approximate convex decomposition for 3d meshes with collision-aware concavity and tree search". In: *ACM Transactions on Graphics (TOG)* 41.4 (2022), pages 1–18.

[32] Trafikverket. *BVS 1585.005 - Typsektioner för banan.* 2015.

[33] B. N. Whittaker et al. *Rock fracture mechanics. Principles, design and applications.* 1992.